Heterogeneous Catalysis

DOI: 10.1002/anie.200703085

Origin and Dynamics of Oxygen Storage/Release in a Pt/Ordered CeO_2–ZrO_2 Catalyst Studied by Time-Resolved XAFS Analysis**

*Takashi Yamamoto, Akane Suzuki, Yasutaka Nagai, Toshitaka Tanabe, Fei Dong, Yasuhiro Inada, Masaharu Nomura, Mizuki Tada, and Yasuhiro Iwasawa**

CeO_2 and cerium-based materials can store oxygen under excess-oxygen conditions and release it under oxygen-deficient conditions, and owing to the high oxygen storage/release capacity (OSC) they are widely used as promoters of automobile three-way catalysts.[1–8] Toyota research groups found that addition of zirconium cations to CeO_2 dramatically improved the OSC and thermal stability.[9–11] The most efficient CeO_2–ZrO_2 (CZ) material is a CeO_2–ZrO_2 solid solution which has an atomically homogeneous, ordered arrangement of Ce and Zr ions assigned to the κ-$Ce_2Zr_2O_8$ fluorite phase (see the Supporting Information),[12] and the OSC increases with increasing homogeneity of the cation arrangement.[7,13] 89% of the Ce ions in the Pt-promoted κ-$Ce_2Zr_2O_8$ are effective in the oxygen storage/release process, in contrast to the low OSC value of pure CeO_2 (2%).[7,12]

The Pt-promoted κ-$Ce_2Zr_2O_8$ transforms into pyrochlore $Ce_2Zr_2O_7$ under the reducing conditions in the working state (see the Supporting Information). A $Ce_2Zr_2O_{7.5}$ intermediate phase forms on prolonged exposure of $Ce_2Zr_2O_7$ to air at room temperature,[14] but there is no information on the formation of $Ce_2Zr_2O_{7.5}$ during the oxygen storage/release process under working conditions. Oxygen storage/release processes on CZ samples have been characterized by various methods such as temporal analysis of products for Pt/CZ,[15] time-resolved XRD,[16] and thermogravimetric analysis for oxygen release from Pt/κ-$Ce_2Zr_2O_8$.[17] A tetragonal $Ce_2Zr_2O_8$ phase with much lower OSC efficiency (52%) than the present κ-$Ce_2Zr_2O_8$ phase (89%) was also characterized by X-ray absorption fine structure (XAFS) analysis.[13,18] Nevertheless, the previous studies did not focus on the real-time dynamics of CZ samples, which may be most relevant to the OSC function. Both Zr and Ce ions in κ-$Ce_2Zr_2O_8$ are in oxidation state +4 and eight-coordinate.[19] In pyrochlore $Ce_2Zr_2O_7$, Ce ions have oxidation state +3 and eightfold coordination, while Zr ions have oxidation state +4 and are sixfold coordinated.[19–21] In the transformation between κ-$Ce_2Zr_2O_8$ and $Ce_2Zr_2O_7$, Zr sites change the number of coordinated oxygen atoms without any change in valence, whereas Ce sites change their valence without changing their coordination number.

We have succeeded in characterizing electronic and structural transformations of the Pt-promoted CZ catalyst with an ordered arrangement of Ce and Zr ions during the oxygen storage/release processes at 573–773 K by real-time energy-dispersive XAFS. Figure 1 shows a series of time-resolved Ce L_3-edge energy-dispersive X-ray absorption near-edge structure (XANES) spectra of Pt/$Ce_2Zr_2O_8$ in an oxygen-release process at 573 K under 12.4 kPa H_2. The virgin Pt/$Ce_2Zr_2O_8$ sample gives typical doublet white lines characteristic of Ce^{4+} species in $Ce_2Zr_2O_8$[16,22,23] and CeO_2.[24] On H_2 dosing the doublet transformed into a singlet and the edge position shifted to lower energy, and after 20 s the spectrum became identical to a typical spectrum of Ce^{3+} species in $Ce_2Zr_2O_7$. The serial XANES spectra exhibited an isosbestic point, except for the first 0.9 s and the last 2 s of the transformation, which indicates that the majority of κ-$Ce_2Zr_2O_8$ transforms directly into pyrochlore $Ce_2Zr_2O_7$. This agrees with temperature-programmed reduction of $Ce_2Zr_2O_8$ with H_2, which showed only a peak around 510 K. After removal of the gas phase, the $Ce_2Zr_2O_7$ was exposed to 12.4 kPa O_2 at 573 K, which recovered the initial doublet feature.

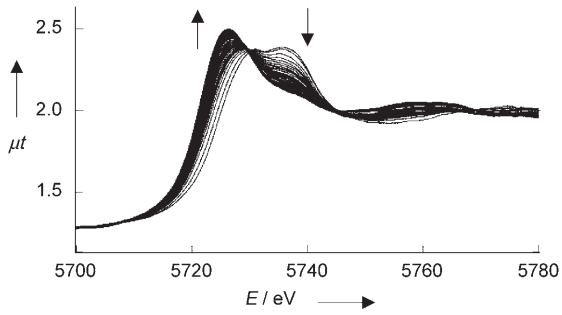

Figure 1. Serial energy-dispersive XANES spectra at the Ce L_3 edge during oxygen release of Pt/$Ce_2Zr_2O_8$ at 573 K. $\mu t = -\ln(I/I_0)$.

[*] Dr. T. Yamamoto, Dr. A. Suzuki, Dr. M. Tada, Prof. Dr. Y. Iwasawa
Department of Chemistry, Graduate School of Science
The University of Tokyo, Hongo, Bunkyo-ku, Tokyo 113-0033 (Japan)
Fax: (+81) 3-5800-6892
E-mail: iwasawa@chem.s.u-tokyo.ac.jp
Dr. Y. Nagai, T. Tanabe, Dr. F. Dong
Toyota Central R&D Labs. Inc.
Nagakute, Aichi 480-1192 (Japan)
Dr. Y. Inada, Prof. Dr. M. Nomura
Photon Factory, Institute of Materials Structure Science
High Energy Accelerator Research Organization (KEK)
Tsukuba, Ibaraki 305-0801 (Japan)

[**] This work has been performed with approval of PF PAC (Proposal No. 2001G316, 2003G294). XAFS = X-ray absorption fine structure.

Supporting information for this article is available on the WWW under http://www.angewandte.org or from the author.

To evaluate time profiles of the fractions of Ce^{4+} and Ce^{3+}, the energy-dispersive XANES spectra were analyzed by a linear combination with the formula $X_{obs} = C_1X_1 + C_2X_2$, where X_{obs}, X_1, X_2, C_1 and C_2 represent observed XANES, XANES spectra of $Ce_2Zr_2O_8$ (Ce^{4+}) and $Ce_2Zr_2O_7$ (Ce^{3+}), and fractions of Ce^{4+} and Ce^{3+}, respectively.[25,26] The sum of C_1 and C_2 was constant at unity. The fractions of Ce^{3+} and Ce^{4+} species in the oxygen storage/release processes were plotted as a function of exposure time to O_2 or H_2 at 573, 673, and 773 K (Figure 2). The Ce^{4+} fraction in the oxygen-release process rapidly decreased above 673 K and the rate depended on the temperature, whereas the temperature dependency was not remarkable in the oxygen-storage processes at 573–773 K.

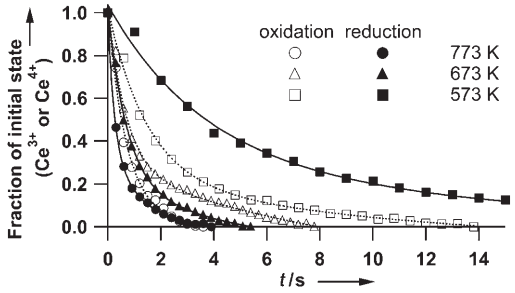

Figure 2. Time profiles of the fractions of Ce^{3+} and Ce^{4+} in $Pt/Ce_2Zr_2O_x$ ($x = 7$ or 8) during oxygen storage and release, respectively (± 0.03).

The change in Ce valence at 773 K was almost complete after 1 s (90 % of the Ce ions in oxygen release and 80 % in oxygen storage). Thus, oxygen storage/release is a dynamic event involving whole $Ce_2Zr_2O_x$ nanoparticles with dimensions of 200 nm.

To elucidate the dynamics of Zr–O bond formation and breaking in the CZ solid solution during the OSC function, changes in the coordination sphere around Zr ions were monitored by energy-dispersive XANES and extended X-ray absorption fine structure (EXAFS) at the Zr K edge with a time resolution of 2 ms. Figure 3a shows real-time k^3-weighted energy-dispersive EXAFS Fourier transforms for $Pt/Ce_2Zr_2O_8$ in the oxygen-release process at 773 K. Rietveld analysis of pyrochlore $Ce_2Zr_2O_7$ reveals that the bond length and coordination number of the Zr–O pair are 0.20995 nm and six, respectively,[21] while κ-$Ce_2Zr_2O_8$ has Zr–O bond lengths of 0.173–0.274 nm (av 0.221 nm) in compulsive eight-fold coordination.[19] The changes in the coordination number and Zr–O distance were successfully analyzed by real-time EXAFS analysis, although the obtained distances are averaged. The results at 773 K are plotted in Figure 3b and c. In the oxygen-storage process the coordination number and bond length slowly increased over 5 s to 7.0 and 0.214 nm, respectively, with only a small increase during the first 1 s (in contrast with the change in Ce valence), and $Ce_2Zr_2O_7$ transformed into $Ce_2Zr_2O_8$ after 6 s. Temperature-programmed oxidation of $Ce_2Zr_2O_7$ with O_2 showed double peaks around 400 and 600 K. Thus, it is likely that the oxygen-storage process proceeds via an intermediate $Ce_2Zr_2O_{7.5}$ phase, but the existence of $Ce_2Zr_2O_{7.5}$ is unlikely at 773 K

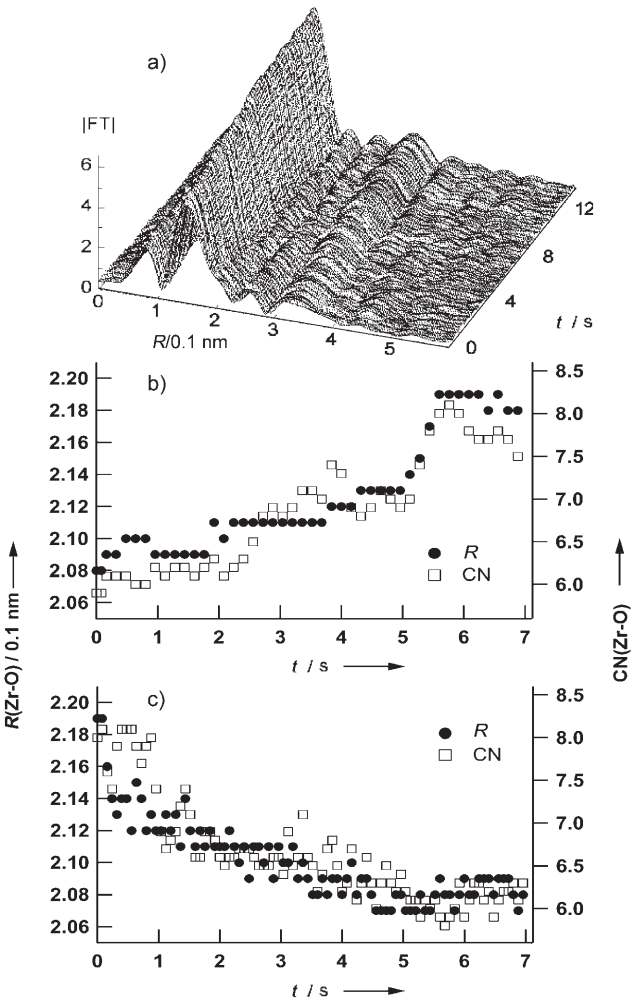

Figure 3. a) Serial k^3-weighted energy-dispersive EXAFS Fourier transforms at the Zr K edge for $Pt/Ce_2Zr_2O_8$ in the oxygen-release process at 773 K. b and c) Time profiles of the coordination number (CN) and Zr–O distance (R) in the oxygen-storage (b) and -release processes (c) at 773 K. $R \pm 0.002$ nm. CN ± 0.7.

due to its instability. In the oxygen-release process the coordination number decreased from eight to seven in 1 s, followed by a gentle decrease to six, while the bond length shortened from 0.220 to 0.214 nm rapidly within 1 s, followed by a continuous decrease to 0.208 nm as the onset of the change in the coordination number. The fast event in the initial stage of oxygen release may be synchronized with the fast valence change of Ce^{4+} ions in Figure 2, but the degrees of change in 1 s differ greatly between Ce valence (90 %) and Zr–O bonding (50 %).

The fractions of $Ce_2Zr_2O_8$ and $Ce_2Zr_2O_7$ during the oxygen-storage and -release processes at 573, 673, and 773 K were also determined by a linear combination analysis of their energy-dispersive XANES spectra at the Zr K edge (Figure 4 and Supporting Information). Temperature dependence was observed in the oxygen-release process, whereas it was not so pronounced in the oxygen-storage process. The most striking aspect is the remarkable difference in the oxidation/reduction rates between Zr and Ce sites. For

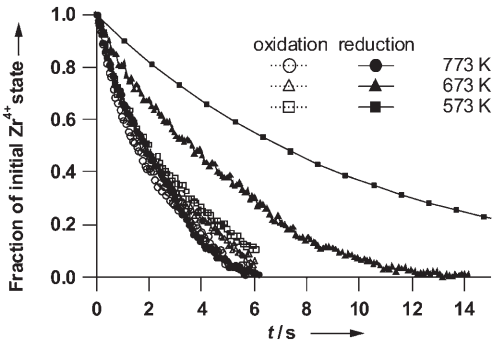

Figure 4. Time profiles of the fractions of $Ce_2Zr_2O_7$ and $Ce_2Zr_2O_8$ during the oxygen-storage and -release processes of Pt/$CeZrO_x$ determined by Zr K-edge energy-dispersive XANES.

example, the Ce L_3-edge XANES analysis for the oxygen-release process demonstrated that 90% of Ce^{4+} ions in $Ce_2Zr_2O_8$ were reduced within 1 s at 773 K, whereas it took 4 s for 90% transformation at Zr sites in the Zr K-edge XANES analysis. The sample amount utilized for the Zr K-edge XAFS measurements was three times greater than that for the Ce L_3-edge XAFS measurements, but volumetric analysis of oxygen uptake indicated that the effect of sample amounts on the OSC rate was not significant (see the Supporting Information).

Based on the time-resolved XAFS analysis, we conclude that the electronic and structural transformations at Ce and Zr sites during the oxygen storage/release processes are not synchronized with each other in the solid solution. In both the oxygen-storage and –release processes, the valence of Ce sites change first, and then structural transformation occur at Zr sites with making or breaking of Zr–O bonds. The oxygen-storage and -release processes monitored by thermogravimetric analysis (Supporting Information) refer to the slower event at Zr sites. To better understand the dynamic oxygen-storage and -release behaviors, we estimated activation energies for the OSC function at both Ce and Zr sites from the dynamic XAFS data at 573–773 K (Supporting Information), and the results are summarized in Table 1. The dynamics at Zr sites observed by energy-dispersive XAFS involve changes in local structure and number of coordinated oxygen atoms, as well as oxygen diffusion. The activation energy for the oxygen-storage process at Zr sites was estimated to be as low as 4 kJ mol^{-1}. The same value was also determined from energy-dispersive EXAFS analysis of the coordination number and Zr–O distance (Table 1). On the other hand, the activation energy for the oxygen-release process at Zr sites is 43 kJ mol^{-1}, that is, ten times larger than that for the oxygen-storage process. A similar value of 36 kJ mol^{-1} was determined from the EXAFS analysis. The activation energy for the oxygen-release process was the same at Zr and Ce sites, as expected for the solid solution. However, the activation energy of 20 kJ mol^{-1} for the oxygen-storage process at Ce sites is completely different from that of 4 kJ mol^{-1} for Zr sites, and this reflects the very different time profiles in Figure 2 (Ce valence) and Figure 3b (Zr–O bonding). The activation energy of 110–161 kJ mol^{-1} for oxygen diffusion in bulk $Ce_2Zr_2O_8$, estimated from electrical conductivity measurements,[27,28] is much larger than the present values evaluated by real-time XAFS analysis. The reason for the difference is not clear, but the XAFS data are more directly relevant to Ce and Zr sites on the molecular scale.

Table 1: Activation energies and rate constants in the oxygen-storage and -release processes of Pt/CZ at 573–773 K.

	Activation energy [kJ mol^{-1}]		k [s^{-1}][a]	
	Oxygen storage	Release	Oxygen storage	Release
Zr	4 (4)[b]	43 (36)[b]	0.46	0.39
Ce	20	43	1.39	2.17

[a] From initial rate at 773 K. [b] Estimated from energy-dispersive EXAFS analysis.

We propose the following factors for explaining the different dynamics at Ce and Zr sites: 1) electron-conducting property of the CZ sample,[27,28] 2) oxygen diffusion via vacant O_h sites in the CZ lattice, 3) valence fluctuation at Ce sites,[29] and 4) charge redistribution due to a change in the lattice constant on modification of the Ce–O distance. In the oxygen-release process from κ-$Ce_2Zr_2O_8$, for example, after H_2 adsorption and spillover at the surface,[30] lattice oxygen at T_d sites moves to O_h sites (Supporting Information) and diffuses in the whole bulk through the vacant O_h sites. In the CZ solid solution, pronounced mixing between Ce 4f and O 2p orbitals and strong overlap between Ce 4f and Ce 5d orbitals are expected,[24] and the oxygen-defect structure ($Ce_2Zr_2O_x$) bestows intervalent character on Ce ions,[21] which may cause valence fluctuation at the Ce sites during the first stage of OSC processes. The Ce valence may be redistributed during the course of oxygen release due to a change in the lattice constant. Oxygen migration to the O_h sites may be relevant to the rapid valence changes at Ce sites in the both oxygen-storage and -release processes. The initial event of site movement is initiated by Zr–O bond breaking at the T_d sites, which is mainly responsible for the activation energy in the oxygen-release process. The first step in oxygen storage is O_2 dissociation at the surface, and the resultant oxygen atoms diffuse to the bulk O_h sites. The fast valence change of Ce ions and the moderate structural change around Zr ions are suggested to be responsible for the high OSC of the ordered CeO_2–ZrO_2 phases. The mechanism of the observed asynchronous behavior is still unclear and further study is needed for a solid explanation. The present XAFS study evidenced the dynamics and roles of Ce and Zr ions in the industrially relevant Pt/CeO_2–ZrO_2 catalyst for the first time, and suggests promising application of dynamic XAFS to a variety of mixed-oxide catalysts.

Experimental Section

The CeO_2-ZrO_2 solid solution (molar Ce:Zr ratio 1:1) was prepared by coprecipitation from aqueous solutions of $Ce(NO_3)_3$ and $ZrO(NO_3)_2$. The obtained precipitate was reduced at 1473 K for 4 h with pure CO, and then calcined in air at 773 K for 3 h. Pt (1.0 wt%) was supported on CeO_2–ZrO_2 by impregnation with an aqueous solution of $[Pt(NH_3)_2(NO_3)_2]$ and subsequent calcination at 773 K for 3 h in

air. The obtained crystalline $Pt/Ce_2Zr_2O_8$ was the κ-phase according to XRD.

Energy-dispersive XAFS is an in situ characterization technique to monitor X-ray intensities over the whole energy range simultaneously with subsecond time resolution.[25,26,31–33] Time-resolved energy dispersive XAFS spectra at the Ce L_3 edge and Zr K edge were measured by Bragg-type polychromators at NW2 in PF (Supporting Information). The time-resolved XAFS spectra for oxygen storage/release processes were recorded in a homemade in situ cell every 2 ms for Zr K-edge XAFS and every 300 ms for Ce L_3-edge energy-dispersive XAFS under 12.4 kPa of O_2 or H_2 in the temperature range 573–773 K. The structural parameters were determined by a curve-fitting procedure in R space by using the FEFFIT program with multiple scattering effects.[34]

Received: July 11, 2007
Revised: August 22, 2007
Published online: October 30, 2007

Keywords: cerium · EXAFS spectroscopy · kinetics · time-resolved spectroscopy · zirconium

[1] H. S. Gandhi, A. G. Piken, M. Shelef, R. G. Delesh, *SAE Paper* **1976**, 760201.
[2] H. C. Yao, Y. F. Yu Yao, *J. Catal.* **1984**, *86*, 254 – 265.
[3] a) JP 1290398, **1985**; b) JP 116741, **1988**.
[4] S. Matsumoto, *Toyota Tech. Rev.* **1994**, *44*, 12 – 17.
[5] J. Kašpar, P. Fornasiero, M. Graziani, *Catal. Today* **1999**, *50*, 285 – 298.
[6] R. Di Monte, J. Kašpar, *J. Mater. Chem.* **2005**, *15*, 633 – 648.
[7] M. Sugiura, *Catal. Surv. Asia* **2003**, *7*, 77 – 87.
[8] S. I. Matsumoto, *Catal. Today* **2004**, *90*, 183 – 190.
[9] M. Ozawa, M. Kimura, A. Isogai, *J. Alloys Compd.* **1993**, *193*, 73 – 75.
[10] F. Fally, V. Perrichon, H. Vidal, J. Kašpar, G. Blanco, J. M. Pintado, S. Bernal, G. Colon, M. Daturi, J. C. Lavalley, *Catal. Today* **2000**, *59*, 373 – 386.
[11] S. Rossignol, Y. Madier, D. Duprez, *Catal. Today* **1999**, *50*, 261 – 270.
[12] A. Suda, Y. Ukyo, H. Sobukawa, M. Sugiura, *J. Ceram. Soc. Jpn.* **2002**, *110*, 126 – 130.
[13] Y. Nagai, T. Yamamoto, T. Tanaka, S. Yoshida, T. Nonaka, T. Okamoto, A. Suda, M. Sugiura, *Catal. Today* **2002**, *74*, 225 – 234.
[14] T. Sasaki, Y. Ukyo, A. Suda, M. Sugiura, K. Kuroda, S. Arai, H. Saka, *J. Ceram. Soc. Jpn.* **2003**, *111*, 382 – 385.
[15] Y. Sakamoto, K. Kizaki, T. Motohiro, Y. Yokota, H. Sobukawa, M. Uenishi, H. Tanaka, M. Sugiura, *J. Catal.* **2002**, *211*, 157 – 164.
[16] J. A. Rodriguez, J. C. Hanson, J. Y. Kim, G. Liu, A. Iglesias-Juez, M. Fernández-García, *J. Phys. Chem. B* **2003**, *107*, 3535 – 3543.
[17] T. Tanabe, A. Suda, C. Descorme, D. Duprez, H. Shinjoh, M. Sugiura, *Stud. Surf. Sci. Catal.* **2001**, *138*, 135 – 144.
[18] S. Lemaux, A. Bensaddik, A. M. J. van der Eerden, J. H. Bitter, D. C. Koningsberger, *J. Phys. Chem. B* **2001**, *105*, 4810 – 4815.
[19] H. Kishimoto, T. Omata, S. Otsuka-Yao-Matsuo, K. Ueda, H. Hosono, H. Kawazoe, *J. Alloys Compd.* **2000**, *312*, 94 – 103.
[20] J. B. Thomson, A. R. Armstrong, P. G. Bruce, *J. Solid State Chem.* **1999**, *148*, 56 – 62.
[21] T. Sasaki, Y. Ukyo, K. Kuroda, S. Arai, S. Muto, H. Saka, *J. Ceram. Soc. Jpn.* **2004**, *112*, 440 – 444.
[22] S. H. Overbury, D. R. Huntley, D. R. Mullins, G. N. Glavee, *Catal. Lett.* **1998**, *51*, 133 – 138.
[23] A. Norman, V. Perrichon, A. Bensaddik, S. Lemaux, H. Bitter, D. Koningsberger, *Top. Catal.* **2001**, *16*, 363 – 368.
[24] A. Bianconi, A. Marcelli, H. Dexpert, R. Karnatak, A. Kotani, T. Jo, J. Petiau, *Phys. Rev. B* **1987**, *35*, 806 – 812.
[25] a) A. Yamaguchi, T. Shido, Y. Inada, T. Kogure, K. Asakura, M. Nomura, Y. Iwasawa, *Catal. Lett.* **2000**, *68*, 139 – 145; b) A. Yamaguchi, T. Shido, Y. Inada, T. Kogure, K. Asakura, M. Nomura, Y. Iwasawa, *Bull. Chem. Soc. Jpn.* **2001**, *74*, 801 – 808.
[26] C. Lamberti, C. Prestipino, F. Bonino, L. Capello, S. Bordiga, G. Spoto, A. Zecchina, S. D. Moreno, B. Cremaschi, M. Garilli, A. Marsella, D. Carmello, S. Vidotto, G. Leofanti, *Angew. Chem.* **2002**, *114*, 2447 – 2450; *Angew. Chem. Int. Ed.* **2002**, *41*, 2341 – 2344.
[27] G. Chiodelli, G. Flor, M. Scagliotti, *Solid State Ionics* **1996**, *91*, 109 – 121.
[28] N. Izu, H. Kishimoto, T. Omata, T. Yao, S. Otsuka-Yao-Matsuo, *Sci. Technol. Adv. Mater.* **2001**, *2*, 443 – 448.
[29] S. Arai, S. Muto, T. Sasaki, K. Tatsumi, Y. Ukyo, K. Kuroda, H. Saka, *Solid State Commun.* **2005**, *135*, 664 – 667.
[30] a) N. Hickey, P. Fornasiero, J. Kašpar, J. M. Gatica, S. Bernal, *J. Catal.* **2001**, *200*, 181 – 193; b) A. Norman, V. Perrichon, *Phys. Chem. Chem. Phys.* **2003**, *5*, 3557 – 3564.
[31] B. S. Clausen, H. Topsøe, R. Frahm, *Adv. Catal.* **1998**, *42*, 315 – 344.
[32] M. A. Newton, A. J. Dent, J. Evans, *Chem. Soc. Rev.* **2002**, *31*, 83 – 95.
[33] a) A. Suzuki, Y. Inada, T. Chihara, M. Yuasa, M. Nomura, Y. Iwasawa, *Angew. Chem.* **2003**, *115*, 4943 – 4947; *Angew. Chem. Int. Ed.* **2003**, *42*, 4795 – 4799; b) A. Suzuki, A. Yamaguchi, T. Chihara, Y. Inada, M. Yuasa, M. Abe, M. Nomura, Y. Iwasawa, *J. Phys. Chem. B* **2004**, *108*, 5609 – 5616.
[34] A. L. Ankudinov, B. Ravel, J. J. Rehr, S. D. Conradson, *Phys. Rev. B* **1998**, *58*, 7565 – 7576.

